RSC Advances



This is an *Accepted Manuscript*, which has been through the Royal Society of Chemistry peer review process and has been accepted for publication.

Accepted Manuscripts are published online shortly after acceptance, before technical editing, formatting and proof reading. Using this free service, authors can make their results available to the community, in citable form, before we publish the edited article. This Accepted Manuscript will be replaced by the edited, formatted and paginated article as soon as this is available.

You can find more information about *Accepted Manuscripts* in the **Information for Authors**.

Please note that technical editing may introduce minor changes to the text and/or graphics, which may alter content. The journal's standard <u>Terms & Conditions</u> and the <u>Ethical guidelines</u> still apply. In no event shall the Royal Society of Chemistry be held responsible for any errors or omissions in this *Accepted Manuscript* or any consequences arising from the use of any information it contains.



Cite this: DOI: 10.1039/c0xx00000x

www.rsc.org/xxxxxx

Page 1 of 12 Journal Name

ARTICLE TYPE

Facile in-situ growth of Fe₃O₄ nanoparticles on hydroxyapatite nanorods for pH dependent adsorption and controlled release of proteins

G. Bharath, a D. Prabhu, b D. Mangalaraj, a C. Viswanathan, a N. Ponpandian * a

Received (in XXX, XXX) XthXXXXXXXX 20XX, Accepted Xth XXXXXXXX 20XX 5 DOI: 10.1039/b000000x

ABSTRACT

A general one-pot hydrothermal process was used to prepare different sized Fe₃O₄ nanoparticles dispersed on the hydroxyapatite nanorods with CTAB as surfactant. It also explores the role of hydrothermal reaction temperature and the surfactant on the crystallinity and formation of rod like morphology of HAp. 10 The obtained nanoparticles are systematically studied by X-ray powder diffraction (XRD), Fouriertransform infrared spectroscopy, Raman spectroscopy, field emission scanning electron microscopy (FESEM) with EDS for elemental mapping, transmission electron microscopy (TEM), Brunauer-Emmett-Teller (BET) nitrogen sorptometry and vibrating sample magnetometer (VSM). The assynthesized Fe₃O₄/HAp nanocomposites are further explored to study the pH dependent protein 15 adsorption and controlled release using hemoglobin (Hb) as model protein. A maximum protein adsorption (Q_0) of 166.67 mg/g is observed for the Fe₃O₄/HAp nanocomposite and it increases to 200.07 mg/g by increasing the concentration of Fe₃O₄ nanoparticles. The pH controlled sustained release process is observed for Hb at various pH values of 4.0, 7.4 and 9.0 in phosphate buffer saline (PBS) solution at room temperature. The maximum protein release was obtained for the lower pH values. The dosage 20 dependent in-vitro cytotoxicity assays are also performed to confirm biocompatibility of the prepared samples.

1. INTRODUCTION

In recent years the synthesis of different morphologies of hydroxyapatite (Ca₁₀(PO₄)₆(OH)₂, HAp) nanostructures have 25 become a topic of extreme interest due to their distinctive properties and potential multifunctional applications. It is an important inorganic bio minerals used for bone and teeth. ^{1,2} The HAp nanostructures are fascinating interest in various other applications like nanomedicine, drug and gene delivery, catalyst, 30 gas sensor, biosensor, tissue engineering, adsorption of heavy metals etc.³⁻⁶ These applications requires a nanoparticles with uniform size and shape to improve their physicochemical and functional properties. Also, the control of size as well as shape is very much essential to improve the surface area of these 35 nanoparticles for adsorption and drug delivery applications. ^{7,8,9} Thus the particle geometry plays a key role in improving the functional properties. The HAp crystal structure includes Ca²⁺, PO₄³⁻ and OH ions, the positively charged Ca²⁺ sites surrounded by negatively charged tetrahedral PO₄³⁻ units and OH⁻ ions

40 occupy columns parallel to the hexagonal axis. The positively charged Ca²⁺ ions are mainly present at a (b)-planes and negatively charged PO₄³⁻ and OH⁻ ions are present in the cplanes. 10 These two different charges of HAp may be responsible for the adsorption. The HAp with high specific surface area is 45 prerequisite for an excellent adsorbent properties like higher uptake and release. 8,9,11 Also, HAp and its nanocomposites prepared by several techniques have excellent biodegradability, osseointegration, bioactivity, and mechanical properties.^{5,12} The ZnO and TiO2 doped HAp nanocomposites exhibit an excellent 50 catalytic activity and degrades the industrial dye from waste water under visible light.¹³ The Ag⁺ ions incorporated HAp nanocomposite enhances the anti-bacterial activity. 14 The lanthanide ions (Eu³⁺ and Eu³⁺/Gd³⁺) incorporated HAp nanorods have potential multifunctional applications like multiple-model 55 imaging agents in magnetic resonance imaging (MRI), computed tomography imaging (CTI) and photoluminescence imaging. 15

Strontium (Sr) -doped calcium polyphosphate (SCPP) has been found to improve bone formation and inhibit bone resorption for artificial bone regenerations.¹⁶ The noble metals (Au, Ag and Pd, etc.) doped HAp nanocomposites shown biocompatibility and it 5 was used as active catalysts. 17 However, very few reports are available for the magnetic nanoparticles incorporated HAp nanocomposites. The magnetic field and magnetic nanoparticles improves the osteoinductivity to accelerate the new bone formation based on these biomaterials. 18-24 A number of magnetic 10 nanoparticles are available such as maghemite (γ-Fe₂O₃), hematite $(\alpha - Fe_2O_3)$ and magnetite (Fe_3O_4) . Among these the magnetite (Fe₃O₄) nanoparticles with cubic inverse spinel structure have been extensively used in various biomedical applications such as cell type recognition, magnetic separation, 15 targeted therapeutics and intercellular imaging due to their nontoxic, biocompatibility and unique magnetic properties. 25,26 The controlled morphology with narrow size distribution of Fe₃O₄ nanoparticles were prepared by several colloidal synthetic processes.27-30

20 The Fe₃O₄ incorporated HAp or HAp/Fe₃O₄ nanocomposites are again a promising biomaterials for targeted drug delivery, orthopaedic, hyperthermia-based anticancer treatments, protein adsorption, gene and DNA delivery, novel magnetic guiding for tissue regeneration, heavy metal adsorptions, reusable biosensor 25 and magnetically recyclable/recoverable catalysts etc. 19,31,32 In general these nanocomposites can be prepared by various methods such as co-precipitation, dip-coating, ultrasonic spray pyrolysis, biomineralization coating, mechanochemical, electrochemical coating and hydrothermal techniques.²⁰ These 30 processes deliver a wide range of morphologies like nanosheets, nanorods, hollow microspheres, hierarchical mesoporous, plate like nanoparticles and nanotubes. 19-24,33-36, Among these, the nanorods exhibit higher specific surface area (SSA) and pore size distributions and it is extensively used as an adsorption of protein 35 and heavy metals from waste water. In general, the cetyltrimethyl ammonium bromide (CTAB) can be used as a soft template for the growth of highly *c-axis* oriented HAp nanorods.³⁷

Herein, we report two different concentrations of Fe₃O₄ nanoparticles dispersed on the HAp nanorods prepared by simple 40 hydrothermal process in the presence of CTAB. The influence of reaction temperature and CTAB on the crystallinity and morphology of the samples were also investigated. The nucleation and growth mechanism was systematically examined and proposed a formation mechanism based on the obtained 45 results. Protein adsorption and desorption studies were performed for the prepared nanocomposites with haemoglobin as model protein. The pH and concentration dependent adsorption experiments were also performed for the as-prepared Fe₃O₄/HAp nanocomposites. The adsorption isotherms for the Fe₃O₄/HAp 50 nanocomposites were further analysed with the existing mathematical models. The pH controlled protein release studies were conducted at different pH values of 4.5 and 7 in phosphate buffer saline (PBS). 38-41, 24

2. EXPERIMENTAL SECTION

55 2.1 Materials

All the reagents and chemicals used in the present investigations

were of analytical or equivalent grade and used without further purification. Calcium chloride dihydrate (CaCl₂.2H₂O), diammonium hydrogen phosphate ((NH₄)₂(HPO₄)), ferrous chloride tetrahydrate (FeCl₂·4H₂O) and ferric trichloridehexahydrate (FeCl₃·6H₂O) were obtained from Sigma-Aldrich and N-Cetyl-N,N,N-trimethyl ammonium bromide (CTAB), ammonium hydroxide (NH₄OH), acetone and ethanol were procured from Himedia, India.

65 2.2 Synthesis of magnetite (Fe₃O₄) and hydroxyapatite (HAp) nanocomposites by hydrothermal process.

superparamagnetic (Fe₃O₄)and hydroxyapatite nanocomposite was prepared by hydrothermal process. In a typical synthesis process, 0.01 M of (NH₄)₂ HPO₄ and 0.1 M of 70 CTAB were dissolved in 10 ml of double distilled water with continues stirring. Then, 0.03 M of CaCl₂.2H₂O was dissolved in 10 ml of water. Further, the CTAB-phosphate solution was added drop wise to the calcium chloride solution and adjusts the pH to 10.5 by adding the ammonium hydroxide (30%) with vigorous 75 stirring for 30 min and it is considered as solution A. The same time, 0.01 M of FeCl₂·4H₂O and 0.015 M of FeCl₃·6H₂O were dissolved in 10 ml of aqueous solution to maintain the molar ratio of 1:1.5 for Fe²⁺ and Fe³⁺and the pH was adjusted by ammonium hydroxide (30%). The resultant solution was mixed with solution 80 A and stirred for 20 min to get the translucent mixed solution. This was further transferred to the Teflon-lined stainless steel autoclave and kept in an oven at 180 °C for 12 h. Then it was cooled down to room temperature naturally andthe supernatant was discarded by decontanation. The final brown 85 colour precipitate was washed several times with ethanol andwater. This was dried at 70°C under vacuum to obtain the Fe₃O₄/HAp nanocomposite. This experimental procedure was adopted to prepare the two different molar concentrations (0.5 and 1 M) of iron oxide on HAp. The samples are represented as 90 Fe₃O₄/HAp-1 for 0.5 mM of Fe₃O₄ on HAp and Fe₃O₄/HAp-2 for 1 mM of Fe₃O₄ on HAp.

2.3 Characterization

The X-ray diffraction (XRD) measurements were carried out at room temperature using a PANalytical X'Pert-Pro diffractometer 95 with Cu K α_1 radiation (λ = 1.5406 Å) over a scanning interval (2θ) from 10 to 70°. The average crystallite sizes were estimated using the Scherrer formula from the X-ray line broadening. The infrared spectrum of the samples was obtained by using a Fourier transform infrared (FTIR) spectrometer (Bruker Tensor 27, 100 Germany). The sample was prepared in a KBr pellet for the investigation within the range of 4000 to 450 cm⁻¹. The morphology of the Fe₃O₄/HAp nanostructures was observed by field emission scanning electron microscopy (FESEM) (FEI Quanta-250 FEG) coupled with EDS spectroscopy and 105 transmission electron microscope (TEM, Hitachi H600) operating at 80 kV. UV-Visible spectral analysis was done by using JoscoV-650 spectrophotometer. The specific surface areas and pore sizes were determined by BET-N2 adsorption for the Fe₃O₄/HApnanocrystals using a micromeritics ASAP 2020 110 surface area analyzer. The magnetic properties were studied using a Lakeshore 7404 vibrating sample magnetometer (VSM) at room temperature.

2.4. In-vitro protein adsorption

Batch mode adsorption experiments were carried out to determine the maximum loading capacity of the protein on nanocomposites. Hemoglobin (Hb) was used as a model protein for the present 5 investigation. The Hb adsorption experiment with various concentrations was executed by the following process. Initial experiments were conducted to evaluate the effect of pH (pH 2-10) for loading the Hb on two different adsorbents (Fe₃O₄/HAp-1 and Fe₃O₄/HAp-2). The experimental processes were conducted 10 separately for the two adsorbents. The powdered nanoparticles of 5 mg were immersed in phosphate buffer saline (PBS) solution with the protein concentration of 2 mL, 500 µg mL⁻¹. The pH of the samples was adjusted between 2 to 10 using 0.1 M HCl and NaOH solutions. All the solutions were shaken at a constant room 15 temperature for 4 hours. The final solution was centrifuged and the supernatant was taken out and measured the UV-vis absorption spectrum at a wavelength of 405 nm. The maximum Hb adsorption was observed at pH 7 for the Fe₃O₄/HAp-1 and Fe₃O₄/HAp-2 samples and it was chosen as the optimum pH for 20 entire successive adsorption experiments. The adsorption studies were performed by varying the protein concentration ranging from 500 to 2500 µg mL⁻¹ at pH 7. The protein adsorption capacity of the nanocomposites was calculated by the following mathematical equations.

$$q_e = \frac{(C_o - C_e)V}{W} \tag{1}$$

Where q_e is the Hb adsorption capacity on unit amount of the nanocomposites (mg/g). The C_o and C_e is the initial Hb concentration and final or equilibrium Hb concentration of protein solution ($\mu g \text{ mL}^{-1}$). V is the volume of Hb solution (mL) and W is the dry weight of the nanocomposites (mg).

2.5. In-vitro pH controlled protein release

The pH dependent controlled release of Hb was carried out by immersing a50 mg of Fe₃O₄/HAp-1 and Fe₃O₄/HAp-2 nanocomposites in 20 ml of Hb in phosphate buffer saline (PBS) solution with the concentration of 2000 μg mL⁻¹ at pH 7. This solution was shaken at room temperature for 4 hand followed by centrifugation and freeze drying to obtain the Hb-Fe₃O₄/HAp-1 and Hb-Fe₃O₄/HAp-2 for drug delivery. The *in-vitro* protein release experiments with various pH values were executed as follows. The Hb loaded nanoparticles of 8 mg was immersed in 8 mL of PBS solution and adjusted the pH values as 4, 7.4 and 9 at room temperature with constant shaking of 120 rpm for 4 h. The 2 ml of Hb release solution was withdrawn for pre-determined intervals and replaced with the same volume and pH of fresh PBS solution. The absorption rate of Hb release was measured by UV-vis absorption spectroscopy at a wavelength of 405 nm.

50 2.6. In-vitro cytotoxicity studies

The cytotoxicity of the Fe_3O_4/HAp nanocomposites was evaluated by MTT (3-(4,5 – dimethylthiahiazol – 2 – yl) – 2,5 – diphenyltetrazolium) assay. The humangastric carcinoma cells 55 (MGC-803) was used for the cell viability studies. The MGC-803 was cultured in a RPMI-1640 medium supplemented with 20%

fetal bovine serum and 2% penicillin-streptomycin for 24 hours at 37°C. The MGC-803 cells were first seeded into 96-well plates with a density of 1×10^4 cells per well and incubated for 48 h. The cells were then treated with different dosage of Fe_3O_4/HAp nanoparticles (50-300 μg mL⁻¹) for 24 h at 37 °C and the untreated cells served as the control. After incubation, the Fe_3O_4/HAp nanocomposites were added into wells at treated with various dosages from 50 to 300 μg mL⁻¹ and co-cultured with cells for 24 hours. The cell viability percentage was calculated by the ratio of absorbance of triplicate readings with control wells and the experiments were repeated three times and the mean viability of the three \pm standard deviation was determined.

3. RESULTS AND DISCUSSION

70 The X-ray diffraction (XRD) patterns were used to analysethe crystalline nature and identify the phases present in the as-XRD nanocomposites. The patterns nanocomposite indicates the dual phases of pure HAp (JCPDS card: No. 09-0432) and Fe₃O₄ (JCPDS card: No. 89-0688), as 75 shown in Fig.1 (a,b). The major diffraction peaks appears at 25.87, 31.42, 32.11, 32.52, 39.62 and 49.42° corresponds to the (002), (211), (112), (300), (202), (310), (222), (213) and (004) crystal planes of HAp and 35.59 and 43.83° for the (311) and (400) crystal planes of Fe₃O₄ respectively. The increase in the 80 concentration of iron oxide notably enhances the relative intensity of (311) plane and there is no significant shift in the peak positions of HAp as shown in Fig.1b.It indicates the incorporation of Fe₃O₄ nanoparticles does not influence the crystalline nature and phase purity of HAp. This clearly confirms 85 the formation of well crystallized hexagonal phase of HAp and cubic spinal phase of Fe₃O₄ without any impurity phases.

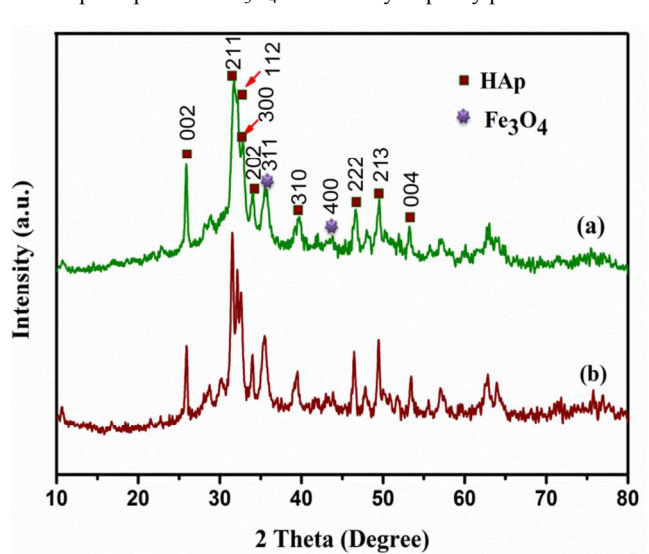


Fig. 1 XRD patterns for (a) $Fe_3O_4/HAp-1$ (0.5 mM of Fe_3O_4) and (b) $Fe_3O_4/HAp-2$ (1 mM of Fe_3O_4) nanocomposites.

90 The FTIR spectra for Fe₃O₄/HAp-1 and Fe₃O₄/HAp-2 nanocomposites are shown in Fig. 2. The adsorption bands observed at 471, 564 and 604 cm⁻¹ corresponds to the bending vibration (v₄) of phosphate groups. The (v₁) vibration of phosphate was observed at 962 cm⁻¹. The absorption bands at 1044 and 1092 cm⁻¹ is attributed to the stretching vibration (v₃) of phosphate group. The sharp absorption peaks at 3570 and 634

cm⁻¹ corresponds to the stretching of an OH band which confirms the incorporation of iron oxide could not affect the OH site of HAp. The broad absorption bands at 3447 and 1639 cm⁻¹ is due to the H₂O present in the synthesized samples.

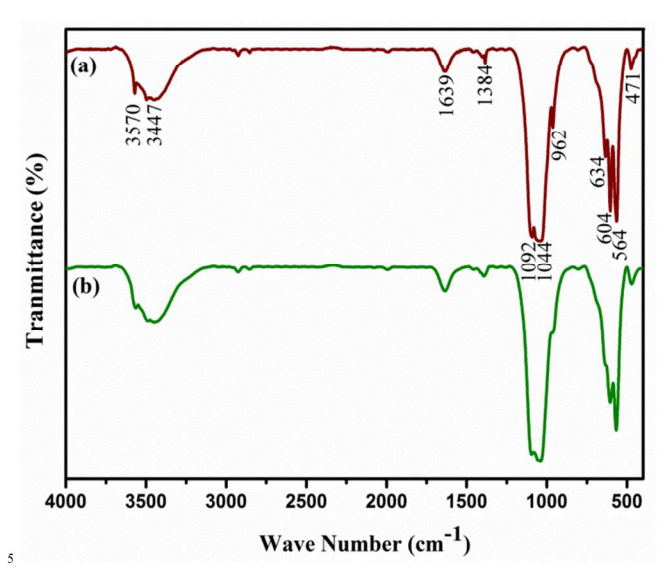


Fig. 2 FTIR spectra for (a) $Fe_3O_4/HAp-1$ (0.5 mM of Fe_3O_4) and (b) $Fe_3O_4/HAp-2$ (1 mM of Fe_3O_4) nanocomposites

Further, it confirms that there is no significant peak shift was observed by increasing the concentration of iron oxide and also the incorporation of Fe₃O₄ does not influences the structure of HAp. The Raman spectroscopy has been used to complete the structural analysis of Fe₃O₄/HAp nanocomposite for the two different concentrations of iron oxide. The magnetite (Fe₃O₄) has a cubic inverse spinel structure with the iron ions (Fe³⁺ and Fe²⁺) occupy interstitial tetrahedral and octahedral sites and the oxygen ions form an *fcc* closed packed structure symbolized as [Fe³⁺]_A. [Fe²⁺Fe³⁺]_BO₄. The magnetite crystal with the space group of *Fd-3m* has five Raman active modes such as A_{1g}, three T_{2g}, and E_g, and four IR active bands (T_{1u}).

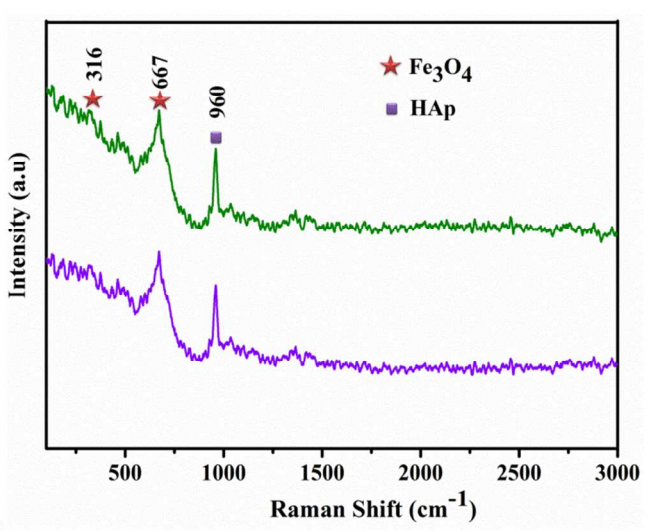


Fig. 3 Raman spectra for (a) Fe $_3$ O $_4$ /HAp-1 (0.5 mM of Fe $_3$ O $_4$) and (b) Fe $_3$ O $_4$ /HAp-2 (1 mM of Fe $_3$ O $_4$) nanocomposites

In the centro-symmetrical space group Fd-3m involves mutual

exclusion of IR and Raman vibrational modes. The Fe^{3+} and O^{2-} ions occupy the T_d and C_{3v} sites respectively and it contribute to the Raman activity, although bivalent iron cations are not directly involved.

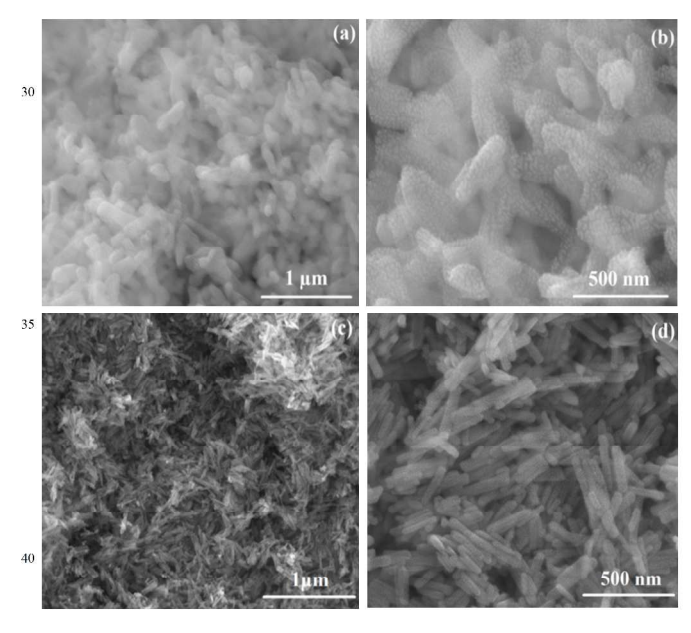


Fig. 4FESEM images for (a,b) $Fe_3O_4/HAp-1$ (0.5 mM Fe_3O_4) and (c,d) $Fe_3O_4/HAp-2$ (1 mM of Fe_3O_4) nanocomposites.

A broad intense peak at 669 cm⁻¹ in Fig. 3(a, b) can be ascribed to 45 the active mode of magnetite A_{1g} and less intense peaks at 540 and 309 cm⁻¹ corresponds to the Raman active modes of T_{2g}, and E_v. In addition, the characteristic band at 960 cm⁻¹assigned to the symmetric stretching (v_1) of the phosphate groups (PO_4^{3-}) . These Raman spectra again confirm the Fe₃O₄ does not influences the 50 crystal structure of Fe₃O₄/HAp nanocomposites. The morphology and elemental compositions of the as-prepared nanocomposites for the two different molar concentrations of Fe₃O₄ (0.5 and 1.0 mM) are investigated by FESEM with EDX mapping and TEM. Initially, the Fe₃O₄ solution is prepared by co-precipitation 55 technique with Fe²⁺ and Fe³⁺ ions in the molar ratio of 1:2 with the total molar ratio of 0.5 mM. Further, the total molar ratio of iron ions $(Fe^{2+} + Fe^{3+})$ was increases to 1 mM. The size of the synthesized Fe₃O₄ nanocrystals increases from 12 to 27 nm by increasing the concentration from 0.5 to 1 mM as shown in 60 supporting information (SI) Fig. 1 (a,b). The concentration of iron ions strongly influences the nucleation growth rate of Fe₃O₄ nanocrystals. The higher concentration of iron ions led to increase the formation of large numbers of seed nucleiand attaching together to form a bigger size Fe₃O₄ nanoparticles. The typical 65 FESEM images of the as-prepared nanocomposites with two different Fe₃O₄ concentrations dispersed on HAp are shown in Fig. 4 (a-d). It shows the 0.5 mM of Fe₃O₄ nanoparticles dispersed on HAp exhibits rod like morphology with slightly ellipsoidal shape. The size of the nanorods in Fig. 4 a&b shows an average 70 diameter and length of 82 and 423 nm respectively for the 12 nm size of Fe₃O₄ nanoparticles homogeneously dispersed on the HAp nanorods.

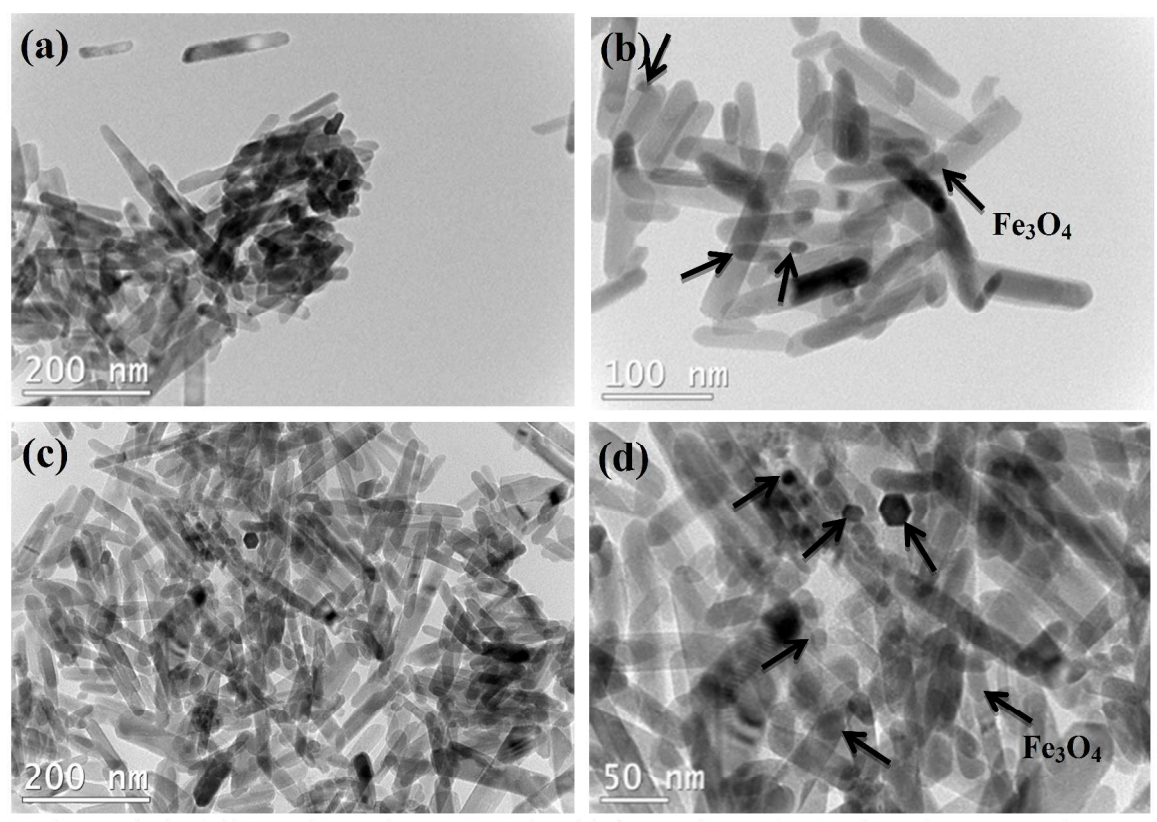


Fig. 5 TEM micrographs for (a,b) Fe₃O₄/HAp-1 (0.5 mM Fe₃O₄) and (c,d) Fe₃O₄/HAp-2 (1 mM of Fe₃O₄) nanocomposites

Figure 4 (c, d) shows the morphology of the 1mM of Fe₃O₄ 5 dispersed on HAp nanocomposite. It shows the rod like morphology with the diameter and length of 39 and 350 nmrespectively. This confirms the large number and higher diameter of Fe₃O₄ nuclei controls the nucleation growth which significantly reduces the diameter and length of the HAp 10 nanorods. Also, the narrow sized Fe₃O₄ nanoparticles are uniformly distributed on the surface of the HAp nanorods. Further, the dispersion of magnetite nanoparticle on the HAp nanorods was clearly visible from the TEM micrographs. Figure 5 (a, b) shows TEM image for 0.5 mM Fe₃O₄ magnetic 15 nanoparticles distributed on the surfaces of the HAp nanorods with smaller size. Moreover, the image in Fig. 5 (c,d) shows the increased size and density of the Fe₃O₄nanoparticles by increasing the Fe₃O₄ concentration to 1 mM and it also distributed on the surface of IIAp nanorods. Further, FESEM-20 EDS and elemental mapping in SI Fig. 2 (a-f) provides the clearer information about distribution of elements in the nanocomposites. It indicates the samples are composed of calcium (Ca), phosphorus (P), oxygen (O) for the HAp template phase and the iron (Fe) for Fe₃O₄ nanoparticles on the surface of HAp 25 nanorods. The increase in iron concentrations from 0.5 to 1.0 mM in the nanocomposites shows the higher numbers of Fe species were dispersed on the surface of HAp as seen in SI Fig. 2(f).

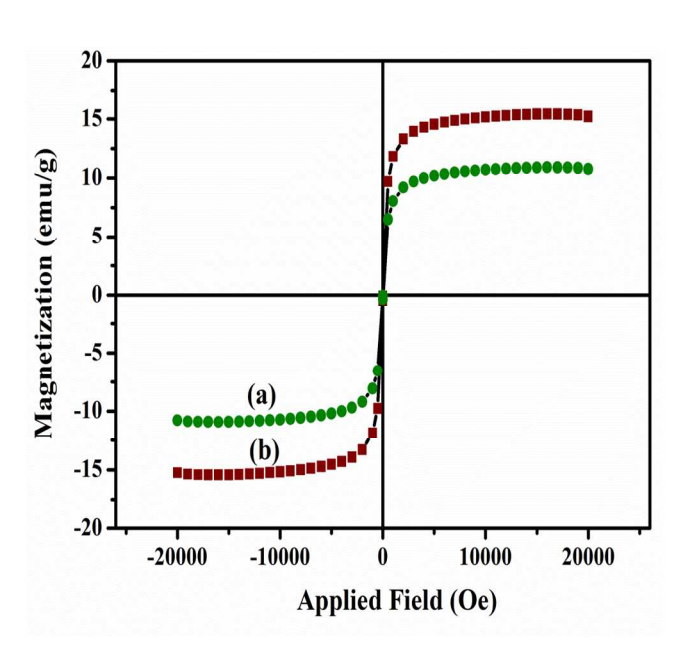
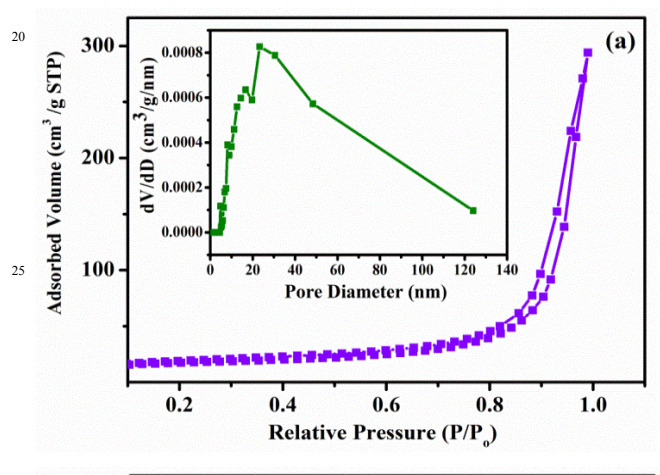
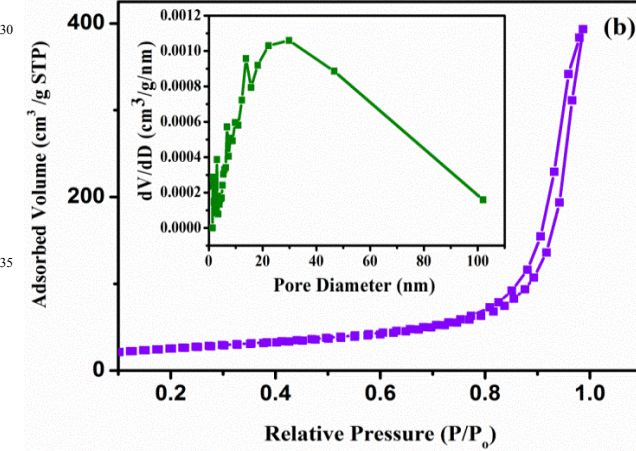


Fig. 6 Magnetic hysteresis loops for (a) Fe₃O₄/HAp-1 (0.5 mM Fe₃O₄), (b) Fe₃O₄/HAp-2 (1.0 mM Fe₃O₄) nanocomposites measured at room temperature.

The magnetic properties of the nanocomposites have also been investigated at room temperature using a vibrating sample magnetometer (VSM) with an applied magnetic field of -2 to +2 KOe.The hysteresis loops for the Fe₃O₄/HAp-1 and Fe₃O₄/HAp-2 nanocomposites in Fig.6 shows the superparamagnetic behaviour

at room temperature. The saturation magnetization (M_s) obtained from the hysteresis loop for the HAp/Fe₃O₄-1 and HAp/Fe₃O₄-1 nanocomposites are 11.5 and 15.5 emu/g respectively with zero coercivity (H_c) . Generally, the increase in the particles size 5 increases the saturation magnetization and coercivity with in the superparamagnetic region. The increase in the average grain size from 12 to 27 nmfor the two different concentrations of Fe₃O₄ nanoparticles grown on the HAp nanorods may be possible increase of the magnetization. The surface area and pore size 10 distribution of HAp/Fe₃O₄nanocomposites are studied by nitrogen physisorption (adsorption-desorption) experiments. Figure 7 (a,b) shows the BET surface area and their corresponding BJH plot for pore size distribution. The adsorption-desorption isotherms confirm a type IV isotherm loop at a relative pressure between 0 15 to 1. Both the samples show mesopores with the pore size distribution of 5 -20 and 15.3 nm for the HAp/Fe₃O₄-1 and HAp/Fe₃O₄-2 nanocomposites using Barrett-Joyner-Halenda (BJH) calculations.





 $_{\rm 40}$ Fig. 7Nitrogen adsorption/desorption isotherms and pore-size distribution (inset) for (a) Fe $_{\rm 3}O_{\rm 4}/{\rm HAp}$ -1 (0.5 mM Fe $_{\rm 3}O_{\rm 4})$ and (b) Fe $_{\rm 3}O_{\rm 4}/{\rm HAp}$ -2 (1 mM of Fe $_{\rm 3}O_{\rm 4})$ nanocomposites.

The obtained specific surface areas forthe HAp/Fe_3O_4-2 and HAp/Fe_3O_4-1 are 91.2 about 80.7 m^2g^{-1} respectively. The higher 45 surface area of HAp/Fe_3O_4-2 can be due to the increase of iron

oxide concentration decreases the grain size of the HAp. This smaller grain size of the HAp enhances the specific surface area. The grain size obtained from XRD and the FESEM images also supports the HAp/Fe₃O₄-2 has small grains as well as the particle sizes required to increase the specific surface area with porous structure.

Nucleation growth mechanism

The formation mechanism of two different concentrations of 55 Fe₃O₄ nanoparticles dispersed on the highly *c-axis* oriented one dimensional HAp nanorods are shown in Fig.8 based on the obtained results. The Fe₃O₄/HAp with two different concentrations of ironoxide (0.5 and 1.0 mM)were prepared by hydrothermal process with CTAB as surfactant. The 60 hydrothermal temperature and CTAB plays a key role in improving the crystallinity and growth. During the growth process, cationic CTAB was dissolved in deionized water and forms spherical shaped micelle. The increase in CTAB concentrations above the critical micelle concentration (CMC) of 65 1 mM, resulting the formation of rod like micelles by the combination of spherical shape CTAB micelles. Subsequently the tetrahedral phosphate (PO43-) ions are attached with the rod shaped tetrahedral CTAB micelle via electrostatic interaction and form a pre-nucleation growth site for the formation of 1D HAp. 70 In addition, the Ca²⁺ ions are also slowly incorporated to the above solution. The Ca2+ ions are deposited and nucleation growth starts along the c-axis and forms the rod shaped hydroxyapatite nanostructures. In addition, the hydrothermal reaction temperature also plays a vital role in the crystallinity and 75 shape evaluation of HAp nanorods. Further, the magnetically induced HAp nanorods are prepared by the addition of certain molar ratios ($Fe^{2+} + Fe^{3+} = 0.5$ and 1 mM) of Fe^{2+} and Fe^{3+} ions (1:2) during the crystallization process of HAp. The increase in the total molar ratio of Fe²⁺ and Fe³⁺ ions from 0.5 to 1 mM 80 increases the size of the synthesized Fe₃O₄ nanocrystals from 12 to 27 nm. This maybe due to the increase in the concentration of iron ions strongly develop the nucleation and growth rate of Fe₃O₄ nanocrystals. The increase in the iron ions concentration from 0.5 to 1 mM increases the formation of a large number of 85 seed nuclei. It provides a largerdiameter of Fe₃O₄ nanoparticles which are dispersed on the 1D HAp nanostructures. The concentration dependent size of the Fe₃O₄ nanoparticles dispersed on the HAp nanorods can be seen through the FESEM and TEMmicrographes and EDX mapping. The concentration 90 dependence of the iron ions are further confirmed from the the change in the intensity of the (311) peak from the XRD pattern and it increases with the increasing concentration. The magnetic properties also changes for the two different concentrationsof Fe₃O₄ nanoparticles. The specific saturation magnetization (M_s) 95 obtained from hysteresis loop increases from 10.6 to 15.5 emu/gm for the 0.5 and 1 mM Fe₃O₄ concentrations.

The larger size of Fe₃O₄nanoparticle dispersed onHAp (HAp/Fe₃O₄-2) nanocomposite shows higher *M*_s due to the surface effect and increased concentration of Fe₃O₄ nanoparticles.

Meanwhile, the larger size Fe₃O₄nanoparticle reduces the nucleation growth of HAp which reduces the size of the HAp

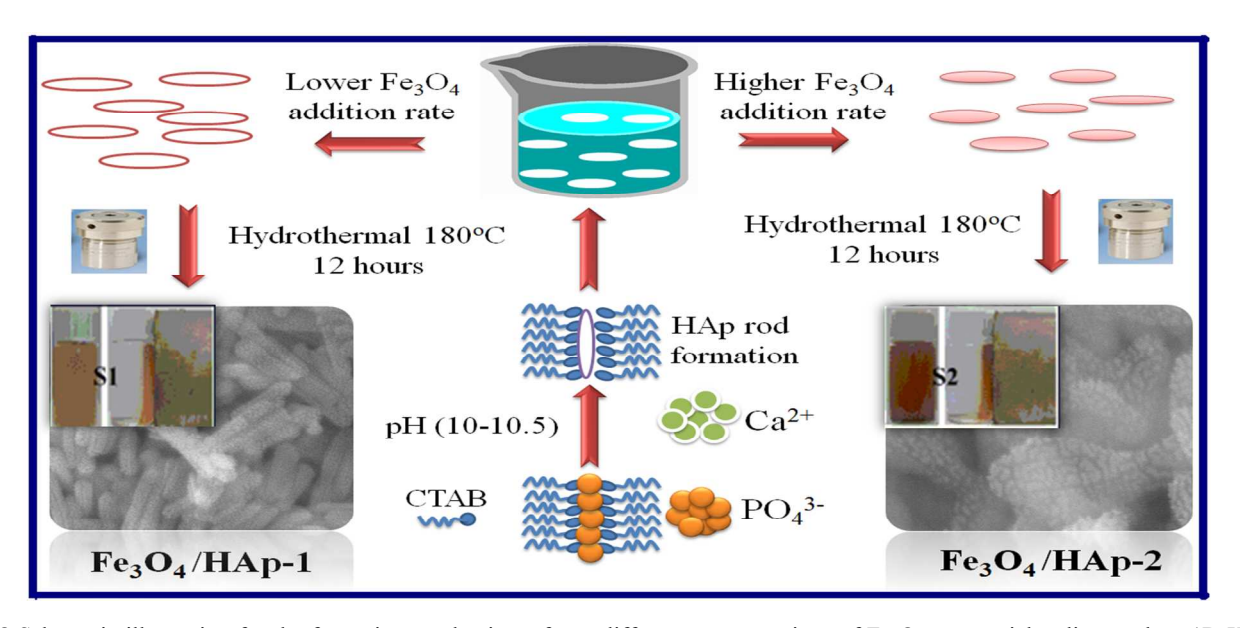


Fig. 8 Schamatic illustration for the formation mechanism of two different concentrations of Fe₃O₄nanoparticles dispersed on 1D HAp nanorods.

nanorods. The size reduction in HAp increases the specific surface area. Thereby, these nanobiomaterials will be efficiently used for various biomedical applications like drug delivery, gene delivery, protein adsorption and potential adsorbents.

3.2. Adsorption behavior of Hemoglobin (Hb) on two different concentrations of ${\rm Fe_3O_4}$ dispersed on HAp nanoparticles

The adsorption behavior of hemoglobin on two different concentrations of Fe₃O₄ nanoparticles dispersed on HAp nanorods have been systematically evaluated based on the effect ofpH, initial concentration of Hb and function of time. The initial pH of the solution is an essential parameter influences the rate of loading of Hb in the nanocomposite.

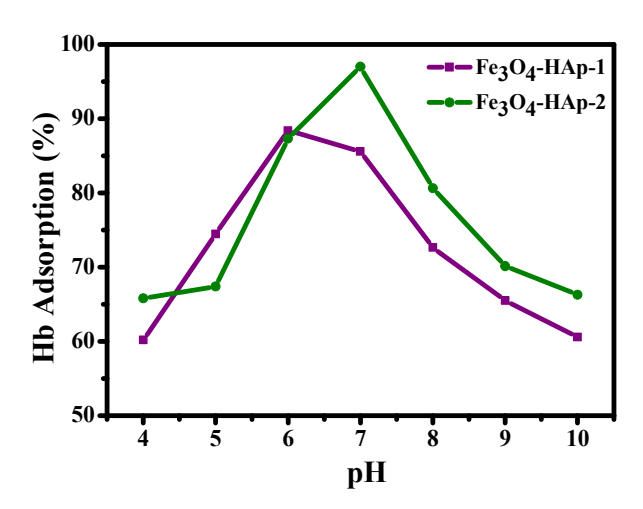


Fig. 9 The pH dependent adsorption (%) of Hemoglobin (Hb) on the Fe₃O₄/HAp-1 and Fe₃O₄/HAp-2 nanocomposites with an initial Hb concentration of 500 μg mL⁻¹ in PBS solution

The Hb is a neutral charge protein and Fe_3O_4/HAp is more positive charged nanoparticles than the pure HAp. The increase in 25 Fe_3O_4 concentrations significantly increases the positive entities and enhances the loading capacity of protein. Adsorption of Hb on Fe_3O_4/HAp -1 and Fe_3O_4/HAp -2 nanocomposites was conducted with the range of pH from 4 to 10 with the initial Hb concentration of $500~\mu g~mL^{-1}$. Figure 9 shows the pH dependent 30 Hb adsorption ability of the nanocomposites with an initial Hb concentration of $500~\mu g~mL^{-1}$ in PBS. The maximum Hb adsorption obtained for the Fe_3O_4/HAp -1 nanocomposite is 85% at pH 6.

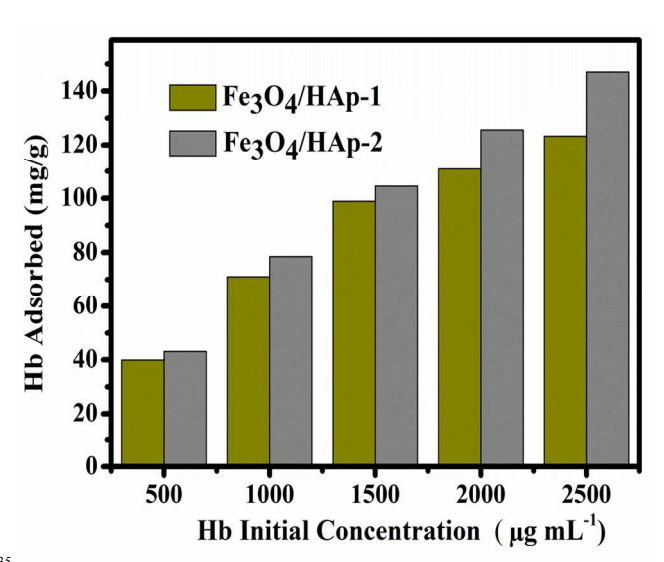


Fig. 10 The Hb loading capacity of the as-prepared Fe₃O₄/HAp-1 and Fe₃O₄/HAp-2 nanocomposites with different initial protein concentration in the range of 500 to 2500 μ g mL⁻¹

40

The other Fe₃O₄/HAp-2 nanocomposite exhibits the maximum adsorption of 95% at pH 7 near the isoelectric point of the protein (pI_(Hb)= 6.8). De Bruin et al. (1969) have already reported that the different pH of 5.75, 6.7 and 7.4 of Hb have different charges of 5 +13, +5 and -1 mV. In the present case, maximum adsorption percentage obtained for the nanocomposites in the pH range of 7-8. Sincethe negative charge of the protein leads to a strong electrostatic interaction with Fe₃O₄/HAp nanocomposites. Meanwhile, the maximum adsorption percentage was obtained at 10 pH 7 for the increased concentration of Fe₃O₄. The electrostatic repulsion occurs between different the Fe₃O₄ nanoparticles in Fe₃O₄/HAp nanocomposite and Hb by increasing the pH to 10 due to the identical net charge and reduces the loading percentage of Hb. The higher percentage of Hb adsorption occurs for the 15 nanocomposites occurs between the pH of 6 -7. Thereby, the further adsorption experiments are conducted with the pH of 7. The Hb loading capacity of the as-prepared nanocomposite was investigated by varying the initial concentrations of Hb from 500 to 2500 µg mL⁻¹ and the experimental results are shown in 20 Fig.10. It shows the loading capacity of the as-prepared nanocomposites increases with increasing initial concentration of Hb. The loading capacity of the Fe₃O₄/HAp-2 nanocomposite reaches a maximum of 150 mg/g for the adsorbed Hb at an initial concentration of 2500 µg mL⁻¹. This adsorption capacity was 25 slightly higher than that of 120 mg/g for the Fe₃O₄/HAp-1 nanocomposite. These results show the as-prepared nanocomposites can exhibit an excellent protein adsorption for the application of nano drug carrier.

Adsorption isotherms

The adsorption isotherms were further analyzed based on the existing mathematical models. These models describe the adsorption capacity of Hb on the nanocomposites and study their nature of adsorption. The characteristic adsorption constants were estimated by fitting the experimental data using Langmuir and Freundlich models to understand the adsorption capacities of Hb on the nanocomposites. The adsorption isotherms of Hb on the two nanocomposites are shown in Fig.11 (a, b) and these data are fitted based on Langmuir and Freundlich isotherms to explain the data adsorption performances. The appearance for the Langmuir and Freundlich isotherm is based on the following two equations

$$\frac{C_e}{q_e} = \frac{1}{Q_0 b} + \frac{C_e}{Q_0} \tag{2}$$

$$\log q_e = \log K_f + \frac{\log C_e}{n} \tag{3}$$

Where q_e and C_e are the equilibrium concentrations of protein (μg mL⁻¹) on adsorbent and in solution respectively. Q_O and b is Langmuir constants related to adsorption capacity and energy of adsorption respectively. The value of Q_O and b indicates themaximum adsorption capacity corresponds to a saturated monolayer of proteins on adsorbent surface. The Freundlich so isotherm model undertakes heterogeneous surface energies in which the energy term in Langmuir equation varies as a function of surface coverage and K_f and I/n are Freundlich constants associated to adsorption capacity and intensity of the adsorption respectively.

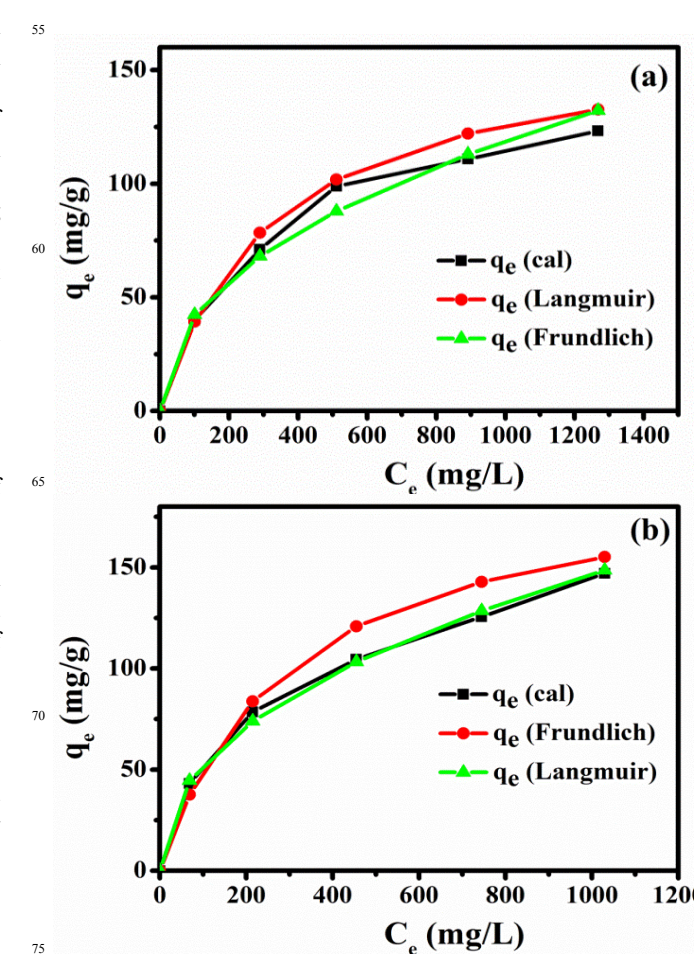


Fig.11Adsorption isotherms of Hb on the nanocomposites with Langmuir and Freundlich models for (a) Fe₃O₄/HAp-1 and (b) Fe₃O₄/HAp-2 in PBS buffer at pH 7.4

The relationship between the adsorption capacity and initial Hb 80 concentration was observed by both Langmuir and Freundlich isotherms. The adsorption isotherms of Hb on Fe₃O₄/HAp-1 and Fe₃O₄/HAp-2 nanocomposites were determined in the concentration range of 500 - 2500 µg mL⁻¹. The observed experimental results in Fig.11shows the increase in the initial 85 concentration of Hb increases adsorption rate on the Fe₃O₄/HAp-1. It is observed that the Hb adsorption is higher for the Fe₃O₄/HAp-2 at the same initial protein concentrations. Both the experimental data are fitted with Langmuir and Freundlich isotherms for the maximum adsorption capacity of Hb on the 90 nanocomposites and the fitted parameters are summarized in Table 1. The correlation coefficient (R^2) of Fe₃O₄/HAp-1 nanocomposite exhibits 0.9972 for Langmuir and 0.9723 for the Freundlich isotherms and the maximum adsorption capacity (Q_a) of the sample is 166.67 mg/g. The correlation coefficient (R^2) of 95 Fe₃O₄/HAp-2 nanocomposite is 0.9923 for Langmuir and 0.9841 for the Freundlich isotherms and the maximum loading capacity (Q_o) of the sample is 200 mg/g. Further, the Langmuir model was used to calculate the Hb adsorption and it indicates the monolayer adsorption with the maximum adsorption occurs for the 100 Fe₃O₄/HAp-2 than that of Fe₃O₄/HAp-1 nanocomposites.

Table 1 Fitted parameters for the Langmuir and Freundlich models of adsorption isotherm for the Hb loaded on $Fe_3O_4/HAp-1$ and $Fe_3O_4/HAp-1$ nanocomposites.

Samples	Langmuir Parameters			Freundlich Parameters		
	R^2	Qo (mg/g)	b (1 mg/g)	R^2	K _F (mg/g)	1/n
Fe ₃ O ₄ /HAp-1	0.9972	166.67	0.0031	0.9723	5.3456	0.4490
Fe ₃ O ₄ /HAp-2	0.9841	200.01	0.0033	0.9946	6.7765	0.4450

Table 2 Summary of the maximum Hb adsorption capacities of different biomaterials

S.No	Biomaterials	Maximum adsorption capacity $Q_O(\text{mg/g})$	Reference	
1	Polyhedral like Hydroxyapatite	164	11	
2	Hydroxyapatite (HAp)/ Fe ₃ O ₄	150	24	
3	HAP porous hollow microspheres	120	39	
4	Hierarchical HAp	177	41	
5	Mesoporous Silica	57	43	
6	Fe ₃ O ₄ @NH ₂	34.51	44	
7	Fe ₃ O ₄ /HAp-1	166.67	Present study	
8	Fe ₃ O ₄ /HAp-2	200.01	Present study	

The regression values of both nanocomposites clearly confirm the 10 experimental data was best fitted for the Langmuir isotherm than that of the Freundlich isotherm. It concludes that the adsorptions of Hb on the nanocomposites may be monolayer adsorption on a surface with homogeneous system. Subsequently, The Hb adsorption capacity of the HAp nanorods was higher than that of 15 the available reported values as presented in Table 2. The adsorption kinetics of Hb on the nanocomposites in Fig.12 shows the protein adsorption process is a time dependent phenomena. Also, the present nanocomposite materials show excellent and fast adsorption rate. The Fe₃O₄/HAp-1 nanocomposite exhibit an 20 adsorption capacity of Hb and the rate of adsorption rapidly increases for the initial 20 min and reach the equilibrium after 25 min. But, in the case of Fe₃O₄/HAp-2 reaches the equilibrium only after 30 min. The maximum adsorption of Hb on the nanocomposites increases with increase in adsorption time. 25 Therefore, the contact and equilibrium times play an important role in the adsorption of proteins and the loading capacity can be

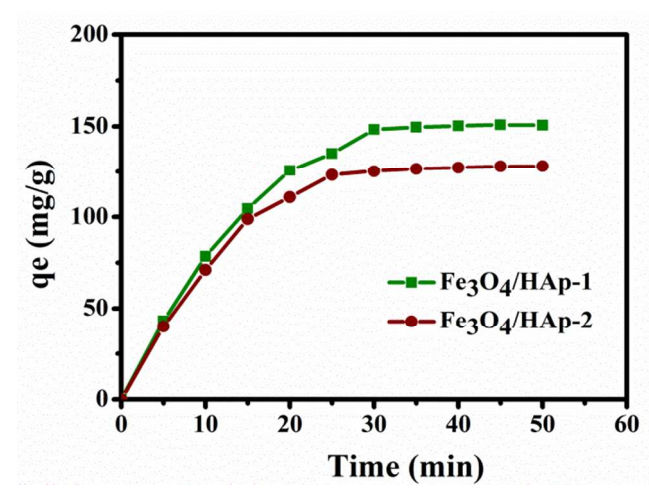


Fig. 12 Adsorption kinetics of Hb on the $Fe_3O_4/HAp-1$ and $_{30}$ $Fe_3O_4/HAp-2$ nanocomposites and the initial concentration of Hb $_{500}$ μg mL⁻¹in PBS buffer at pH 7.4

controlled by varying the time.

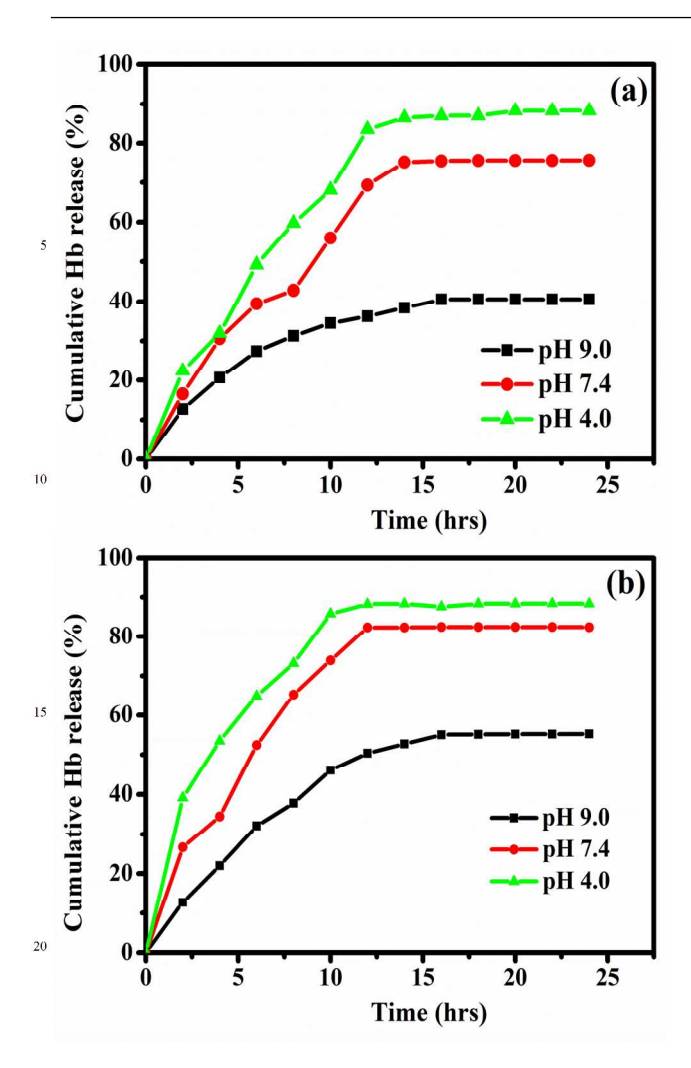


Fig. 13 Cumulative release of hemoglobin (Hb) loaded on (a) Fe₃O₄/HAp-1 and (b) Fe₃O₄/HAp-2 nanocomposites at different 25 initial pH values of 4, 7.4 and 9 in PBS at room temperature.

pH controlled release of Hb

The releasing process was evaluated for the Hb loaded nanocomposites with different pH values in PBS at room temperature. The pH dependent cumulative release ratio (%) is 30 given by the amount of Hb released in PBS solution as a function of time. Three different pH values of 9, 7.4 and 4 are chosen for the pH dependent release of Hb. Figure 13 (a, b) shows the controlled release profile for the IIb loaded Fe₃O₄/IIAp-1 and Fe₃O₄/HAp-2 nanocomposites. The release profile confirms the 35 Hb adsorption of both nanocomposites exhibits a slow and sustained release over a period of 25 hrs. The release percentage of Hb increases for the first 13 hrs for all the pH and attain a steady release till 25 hrs. The amount of Hb release in PBS with the pH of 4.0 is much larger than that of other two pH values of 40 7.4 and 9. Therefore the releasing of Hb from Fe₃O₄/HAp is higher at the acidic condition with the pH of 4 due to the maximum release of calcium and phosphate ions in the range of and 62 mg/L.³⁷Also, the cumulative Hb release percentages(%) in PBS solution with a pH value of 4 reaches a 45 maximum of 87 and 95% corresponds to Fe₃O₄/HAp-1 and Fe₃O₄/HAp-2 Thus, the dissolution respectively.

hydroxyapatite enhances the protein release in PBS at lower pH values. These experiments confirm the Fe_3O_4/HAp nanocomposites are excellent and promising biomaterials as potential pH sensitive drug carrier. The present nanocomposites are an excellent pH sensitive drug carrier and it is potential nano biomaterial for tumour and cancer cell treatments.

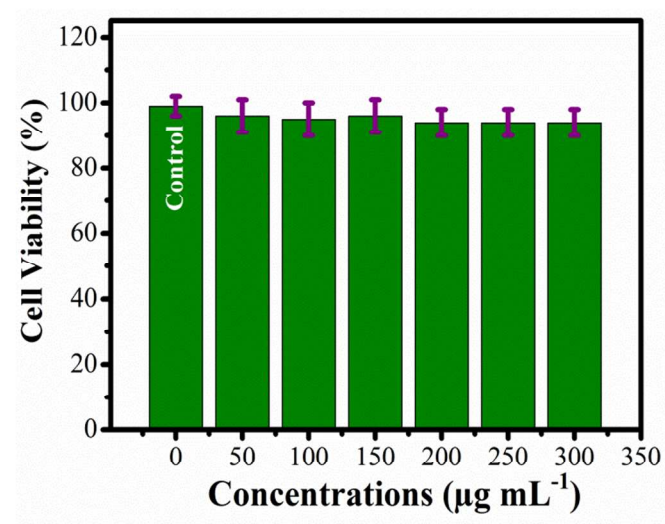


Fig 14. Cell viability of Fe_3O_4/HAp nanocomposite with human ss gastric carcinoma cells (MGC-803) and cell cultured with different dosages of the samples between 50 and 300 μg mL⁻¹.

In-vitro cytotoxicity studies

The dose dependent cytotoxicity analysis for the Fe₃O₄/HAp nanocomposite was performed by using human gastric carcinoma cells (MGC-803). The MTT assay was performed as a colorimetric assay to measure cytotoxicity of the nanocomposites. The observed results for the Fe₃O₄/HAp nanocomposite exhibits 99.5 % of cell viability at the concentration of 50 μg/mL as shown in Fig 14. Interestingly, the higher dosage of 200 μg/mL shows the cell viability of 95.4%. Also, the increasing concentration of Fe₃O₄/HAp nanocomposite between 200 and 300 μg/mL shows the similar cell viability of 95.4%. These results confirm the Fe₃O₄/HAp nanocomposites have modest cytotoxic effect on human gastric carcinoma cells (MGC-803). Hence, we conclude these nanocomposites are biocompatible and promising biomaterials for biomedical applications such as tumor treatment, drug delivery, protein adsorption etc.

4. CONCLUSION

nanorods by *in-situ* hydrothermal process for two different concentrations of Fe₃O₄. The soft template CTAB plays an important role in the formation of nanorods and the reaction temperature improves the crystallinity of Fe₃O₄/HAp nanocomposites. The morphological analysis confirms the dimensions of the HAp nanorod decreases by increasing the concentration of Fe₃O₄. The higher grain size of Fe₃O₄ controls the nucleation growth of HAp. The pH dependent Hb adsorption and sustained release of these nanocomposites clearly indicates their excellent controlled release and the maximum release was obtained at pH 4. The experimental data was best fitted with

70

80

85

100

Langmuir models with the maximum adsorption capacity of 166.67 and 200.07 mg/g corresponding to the Fe₃O₄/HAp-1 and Fe₃O₄/HAp-2 nanocomposites. Thus, these nanocomposites are excellent biomaterials to be useful in biomedical applications 5 such as tumor treatment, drug delivery, protein adsorption *etc*.

ACKNOWLEDGEMENTS

The authors would like to acknowledge the University Grant Commission (UGC), New Delhi, Government of India for the financial support through the major research project and DST-10 PURSE, Government of India for the FESEM facility.

NOTES AND REFERENCES

^aDepartment of Nanoscience and Technology, Bharathiar University, Coimbatore 641 046, India

^bInternational Advanced Research Centre for Powder Metallurgy and 15 New Materials (ARCI), Balapur PO, Hyderabad, India

Corresponding Author

30

40

55

E-mail: ponpandian@buc.edu.in (N. Ponpandian)

- 1. H. Monma and T. Kamiya, *J.mater.Sci.*, 1987, **22**, 4247-4250.
 - K. S. Katti, D. R. Katti and R. Dash, *Biomed. Mater.*, 2008, 3, 034122.
 - D. A. Wahl and J. T. Czernuszka, Eur. Cells Mater., 2006, 11, 43.
- 25 4. S. V. Dorozhkin, J. Mater. Sci., 2007, 42, 1061.
 - G. Xiaohui, W. Wang, W. Guolong, J. Zhang, C. Mao, Y. Deng and H. Xia, New J. Chem., 2011, 35,663–671.
 - G. Bharath, A. Jagadeesh Kumar, K. Karthick, D. Mangalaraj,
 C. Viswanathan and N. Ponpandian, RSC Adv., 2014, 4, 37446-37457.
 - K. Kandori, S. Toshima, M. Wakamura, M. Fukusumi, and Y. Morisada, J. Phys. Chem. B 2010,114,2399–2404.
 - W. H Lee, C. Y. Loo, K. L. Van, A. V. Zavgorodniy and R. Rohanizadeh, R. Soc. Interface, 2012, 9, 918–927.
 - 9. Q. Chao, Z. Ying-Jie, L. Bing-Qiang, X. Y. Zhao, J. Zhao, F. Chen, and J. Wu, *Chem. Eur. J.* 2013, **19**, 5332 5341.
 - C. Chen, Z. Huang, W. Yuan, J. Li, X. Cheng and R. Chi, *CrystEngComm*, 2011, 13, 1632–1637.
 - 11. X. Yu Zhao, Y. J. Zhu, F. Chen, B. Q. Lu and J. Wu, CrystEngComm, 2013, 15, 206–212.
 - J. S. Cho, D. S. Yoo, Y. C. Chung and S. H. Rhee, *J Biomed Mater Res-A.*, 2014, **102**, 456-469.
 - Y. Liu, Q. Yang, J.H. Wei, R. Xiong, C.X. Pan and J. Shi, *Mater. Chem. Phys.*, 2011, 129 654–659.
 - C. S. Ciobanu, F. Massuyeau, L. V. Constantin and D. Predoi, Nanoscale Res Lett., 2011, 6, 613.
 - F. Chena, P. Huang, Y. J. Zhua, J. Wua, D.X.Cui, Biomaterials, 2012, 33, 6447-6455.
 - W. Song, Q. Wang, C. Wan, T. Shi, D. Markel, R. Blaiser and W. Pen J. Riomed. Mater. Ros B. 2011. 98, 255-261
 - 17. A Mocanu G Furtos A Danisteanu G Rapuntean C Prejmerean, M. T. Cotisel, Appli Surf Scien., 2014, 298, 225-235.
 - S. R. Rout, B. Behera, T.K. Maiti and S. Mohapatra, *Dalton Trans.*, 2012, 41, 10777–10783.
 - Y. P. Guo, L. H. Guo, Y. Yao, C. Q. Ning and Y. J. Guo, Chem. Commun., 2011, 47, 12215–12217.
 - C. Huang, Y. Zhou, Z. Tang, X.Guo, Z. Qian and S. Zhou, *Dalton Trans.*, 2011, 40, 5026–5031.
 - D. F. Mercado, G. Magnacca, M.Malandrino, A. Rubert, E. Montoneri, L. Celi, A. B. Prevot, and M. C. Gonzalez, *Appl. Mater. Interfaces.*, 2014, 6, 3937–3946.

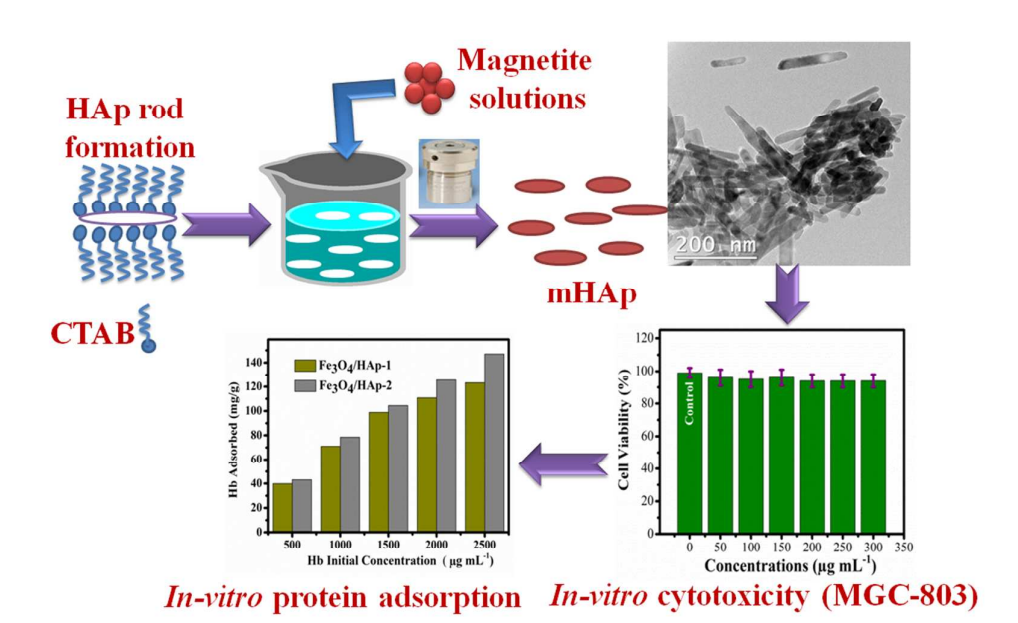
- H. C. Wu, T. W. Wang, M. C. Bohn, F. H. Lin, and M. Spector, Adv. Funct. Mater., 2010, 20, 67–77.
- K. Lin, L. Chen, P. Liu, Z. Zou, M. Zhang, Y. Shen, Y. Qiao,
 X. Liu and J. Chang, *CrystEngComm*, 2013, 15, 2999–3008.
- F. Chen, C. Li, Y. J. Zhu, X. Y. Zhao, B. Q. Lu and J. Wu, Biomater. Sci., 2013, 1, 1074–1081.
- S. Ge, X. Shi, K. Sun, L. Changpeng, C. Uher, J. R. Baker, J. Mark, M. B. Holl, and B.G. Orr, J. Phys. Chem. C., 2009, 113, 13593-13599.
- C. B. Andujar, L. D. Tung and N. T. K. Thanha, *Annu. Rep. Prog. Chem., Sect. A*, 2010, 106, 553–568.
- Demorti, P. Panissod, B. P. Pichon, G. Pourroy, D. Guillon, B. Donnio and S. B. Colin, *Nanoscale*, 2011, 3, 225-232.
- H. Ho, C. P. Tsai, C. C. Chung, C. Y. Tsai, F. R. Chen, H. J. Lin, and C. H. Lai, *Chem. Mater.* 2011, 23, 1753-1760.
- C.A. Demarchi, A. Debrassi, F. C. Buzzi, R. Corr[^] ea, V. C. Filho, C. A. Rodrigues, N. Nedelko, P. Demchenko, A. S. Waniewska, P. Dłu zewski and J. M. Greneche, *Soft Matter*., 2014, 10, 3441–3450.
- X. Luo, S. Liu, J. Zhou and L. Zhang, J. Mater. Chem., 2009, 19, 3538–3545.
- Z. Shan, L. Xianghai, Y. Gao, X. Wang, C. Li, Q. Wu, Anal. Biochem., 2012, 425,125-127.
- 32. E. B. Ansar, M. Ajeesh, Y. Yokogawa, W. Wunderlich, and H. Varma, *J. Am. Ceram. Soc.*, 2012, **95**, 2695-2699.
- X. Guo, L. Yu, L. Chen, H. Zhang, L. Peng, X. Guo and W. Ding, *J. Mater. Chem. B*, 2014, 2, 1760-1763.
- W. Chen, T. Long, Y.J. Guo, Z. A. Zhu and Y. P. Guo, J. Mater. Chem. B, 2014, 2, 1653-1660.
- Y. P. Guo, T. Long, S. Tang, Y. J. Guo and Z. A. Zhu, J. Mater. Chem. B, 2014, 2, 2899-2909.
- K. Lin, L. Xia, J. Gan, Z. Zhang, H. Chen, X. Jiang and J. Chang, *Appl. Mater. Interfaces.*, 2013, 5, 8008-8017.
- M. Salarian, M. Solati-Hashjin, S. Sara Shafiei, A. Goudarzi,
 R. Salarian and A. Nemati, *Materials Science-Poland*, 2009,
 27, 961-971.
- 38. X.Y. Zhao, Y. J. Zhu, F. Chen, B. Q. Lu and J. Wu, *CrystEngComm*, 2013, **15**, 206-212.
- Qi, Y. J. Zhu, B. Q. Lu, X. Y. Zhao, J. Zhao and F. Chen, J. Mater. Chem., 2012, 22, 22642-22650.
- 40. R. Gao, X. Mu, J. Zhang and Y. Tang, *J. Mater. Chem. B*, 2014, **2**,783–792.
- Qi, Y. J. Zhu, B. Q. Lu, X. Y. Zhao, J. Zhao, F. Chen, and J. Wu, Chem. Eur. J., 2013, 19, 5332 – 5341.
- T.Y. Guo, Y.Q. Xia, G.J. Hao, M.D. Song and B.H. Zhang, Biomaterials., 2004, 25, 5905-5912.
- S. Chukhrai, L. F. Atyaksheva, and O. S. Pilipenko, Russian Journal of PhysicalChemistry A, 2011, 85, 890-896
- R. Gao, X. Mu, Y. Hao, L. Zhang, J. Zhang and Y. Tang, J. Mater. Chem. B, 2014, 2, 1733-1741

Graphical Abstract

Facile *in-situ* growth of Fe₃O₄ nanoparticles on hydroxyapatite nanorods for pH dependent adsorption and controlled release of proteins

G. Bharath, D. Prabhu, D. Mangalaraj, C. Viswanathan, N. Ponpandian*

The magnetic hydroxyapatite nanostructures were prepared by hydrothermal techinique and studied their protein adsorption and *in-vitro* cytotoxicity in humen MGC-803 cell.



^aDepartment of Nanoscience and Technology, Bharathiar University, Coimbatore 641 046, India

^bInternational Advanced Research Centre for Powder Metallurgy and New Materials (ARCI), Balapur PO, Hyderabad 500 005, India